Heliyon 10 (2024) e39898

Contents lists available at ScienceDirect

Heliyon

journal homepage: www.cell.com/heliyon

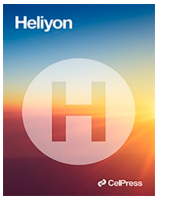

Research article

Nb(V)-containing saponite: A versatile clay for the catalytic degradation of the hazardous organophosphorus pesticide paraoxon under very mild conditions

Stefano Marchesi [a], Stefano Econdi [b,c], Geo Paul [a], Fabio Carniato [a], Leonardo Marchese [a], Matteo Guidotti [b,*], Chiara Bisio [a,b,**]

[a] Dipartimento di Scienze e Innovazione Tecnologica, Università del Piemonte Orientale, Viale Teresa Michel 11, 15121, Alessandria, AL, Italy
[b] CNR-SCITEC Istituto di Scienze e Tecnologie Chimiche "Giulio Natta", Via C. Golgi 19, 20133, Milano, MI, Italy
[c] Dipartimento di Chimica, Università degli Studi di Milano, Via C. Golgi 19, 20133, Milano, Italy

ARTICLE INFO

Keywords:
Saponite clay
Paraoxon
Pesticide
Catalytic abatement
Environmental remediation

ABSTRACT

A synthetic saponite clay containing structural Nb(V) metal centres (NbSAP) was investigated in the abatement of paraoxon-ethyl, an anti-cholinergic organophosphorus pesticide, under mild conditions (neutral pH, room temperature and ambient pressure) in heterogenous phase, without additional basic additives. The material was selected according to its high surface acidity and ease of preparation through a one-step hydrothermal synthesis. The presence of Nb(V) ions played a crucial role in efficiently catalysing the degradation of aggressive chemical substrates. A niobium (V) oxide with very low surface acidity was also tested as a reference material. The study employed a multi-technique approach to monitor the pesticide degradation pathway and by-products formed during abatement experiments in polar non-protic and aqueous solvents. Notably, in water, the concentration of paraoxon-ethyl significantly decreased by 82 % within the first hour of contact with the clay. Additionally, NbSAP demonstrated a good performance after three repeated catalytic cycles and subsequent reactivation.

1. Introduction

Old generation organophosphorus-based compounds (OPPs) have been extensively used for crop protection, because of their high insecticidal and herbicidal activity [1,2]. They still account for over 38 % of global pesticide sales [3]. Highly toxic pesticides with anticholinergic activity, such as chlorpyrifos, diazinon, phorate, malathion, parathion and paraoxon [4], are some of the most widespread OPPs still present in the environment today, even if they are banned in European Union (EU) as well as in several other countries [5–7].

Paraoxon (diethyl *p*-nitrophenyl phosphate) is a hazardous compound and low-to-high levels of exposure have been associated with

* Corresponding author.
** Corresponding author. Dipartimento di Scienze e Innovazione Tecnologica, Università del Piemonte Orientale, Viale Teresa Michel 11, 15121, Alessandria, AL, Italy.
E-mail addresses: stefano.marchesi@uniupo.it (S. Marchesi), stefano.econdi@scitec.cnr.it (S. Econdi), geo.paul@uniupo.it (G. Paul), fabio.carniato@uniupo.it (F. Carniato), leonardo.marchese@uniupo.it (L. Marchese), matteo.guidotti@scitec.cnr.it (M. Guidotti), chiara.bisio@uniupo.it (C. Bisio).

https://doi.org/10.1016/j.heliyon.2024.e39898
Received 21 March 2024; Received in revised form 11 October 2024; Accepted 25 October 2024
Available online 26 October 2024

a wide range of health issues [8–11] including vomiting, impaired vision, convulsions, dyspnea, pulmonary oedema and even death [1,12]. In fact, paraoxon shares a similar molecular structure and phosphorylating mode of action against the nervous system of living organisms with nerve chemical warfare agents (CWAs) [13,14]. For these reasons, it can effectively serve as a simulant of anticholinergic warfare agents in the search for innovative approaches for the decontamination and mitigation of the threat of such highly toxic compounds.

Different methods have been proposed in the literature for the removal and/or degradation of OPPs, such as homogeneous and heterogeneous catalysis, photolysis, adsorption, electrochemical methods, biological and advanced oxidation procedures, phytoremediation and stoichiometric degradation with harsh reactants [4,14–24]. More specifically, some of the methods described in the state-of-the-art for paraoxon abatement, especially at laboratory-scale, envisage the use of alkaline hydrolysis, using piperidine or hydroxylamines and *N*-hydroxy amides in cationic micellar media [7,25], application of specific bacterial strains and enzymes [6,20], enzymatic nanocomposites [26] and hydrogels [27], UV–Vis photodegradation with graphene oxide-based membranes [28], "nano-sponges" based on hydroxylated metal oxides inside carbon nanofibers [29], magnetic nanocatalysts (e.g. from carbon nanotubes) [30], CeO_2 nanoparticles [31], TiO_2-based systems (*e.g.* as films [32], TiO_2/Au/Mg microspheres [33], N-TiO_2/Ag/Ti electrodes [34]), hydrolytic detoxifying processes using hybrid polyoxometalates (POMs) or metal-organic frameworks (MOFs) [35–39], catalytic polymers with different anchored groups (e.g. imidazole, oximes) [40–42], use of waste-derived biocatalysts (e.g. from rice-husk) [22,43,44], reduction with zero-valent Fe nanoparticles [45] and esterolysis in the presence of Cr(III) terephthalate MOFs modified with dialkylaminopyridines complexes [46]. These systems were tested both in batch or in continuous flow systems [20,47–49]. In particular, MOFs are currently materials showing promising performances in terms of capability of degradation and detoxification of hazardous OPPs, under mild conditions and in aqueous solutions/media too [50–52].

Nevertheless, a non-negligible part of these methods display some limitations, such as: reactions in environmentally unfriendly organic or mixed water/organic solvents, use of energy-intensive UV–Vis illumination to generate highly reactive hydroxyl radicals (ROS), high alkaline pH values to promote efficient hydrolysis, relative high amount of homogeneous/heterogenous catalysts compared to OPPs, use of unconventional apparatuses and procedures (e.g. on-design photoreactors), incomplete degradation or formation of secondary pollutants and long reaction times [15,19,20,53,54]. Few studies have focused on the cost-effective and eco-friendly degradation of OPPs in aqueous solution so far and some of them still show drawbacks [55,56].

For example, piperidine in water was used to promote the alkaline hydrolysis of paraoxon-ethyl at pH $>$ 12, with complete degradation only after 2 days [25]. The application of UV/Vis-based photocatalytic systems, which generally employ dedicated equipment and specific processes depending on the (photo)catalyst used, has shown widely spread results in the abatement of paraoxon-ethyl, spanning from partial to near-complete conversion of the pesticide, in either few minutes or several hours [28,32,33]. The relatively expensive materials synthesized and used in these studies normally exploit ROS-mediated photolysis reactions. Nanoparticles with zero-valent iron species were tested in the reduction of paraoxon-ethyl in water, with a maximum degradation of approx. 76 % after 3 h at pH $\approx$ 6 [45]. In several reports, functionalized MOF materials have indeed shown to be active in the hydrolysis of paraoxon, but sometimes the use of peculiar organic/aqueous reaction mixtures (water/acetonitrile) [46] and the presence of basic additives to keep a high pH in the reaction medium ($\geq$ pH 10) were necessary to attain interesting degradation results [57,58].

In the light of the above underlined limitations, the main objective of this research is the use of a synthetic saponite clay containing structural Nb(V) metal centres for the rapid abatement of the organophosphorus paraoxon-ethyl in two polar non-protic solvents (ethyl acetate and dichloromethane) and in aqueous solution under simple and environmentally friendly experimental conditions, without the addition of external basic additives. Synthetic saponite clays have interesting properties as sustainable heterogeneous catalysts, such as controlled chemical composition, high robustness, good chemical versatility, tuneable particles size and surface acidity, low cost and high sorption capacity [59–61]. In the present work, a Nb(V)-containing saponite catalyst was selected because [62–64]: i) the incorporation of Nb(V) sites into the inorganic framework of the clay is able to generate a high Brønsted-type surface acidity, which can be exploited in the catalytic degradation of the selected pesticide; ii) NbSAP samples have already been used as very effective catalysts in the oxidative degradation of blistering agent simulants (2-chloroethyl ethyl sulfide) under mild conditions in the presence of diluted H_2O_2, especially in aqueous phase; iii) NbSAP is prepared using a one-pot approach, where the Nb(V) precursor is added directly at the synthesis stage, eliminating the need for further post-synthesis steps and keeping production costs low. A commercial Nb_2O_5 sample was tested as a reference sample, since it showed excellent performance in organosulfur decontamination in both liquid phase and dry powder form [65]. Furthermore, the regenerability of the Nb(V)-saponite was evaluated for possible applications in multiple catalytic cycles in aqueous phase and, more in general, in pollution remediation strategies.

2. Experimental

All chemicals were purchased from Sigma-Aldrich/Merck KgaA (Darmstadt, Germany), stored at room temperature and used without further purification unless stated otherwise. Commercial Nb_2O_5 powder (cod. 208515) was used as reference catalyst. Prior the use, liquid paraoxon-ethyl (PESTANAL®, analytical standard, cod. 36186) has been stored in a refrigerator at 277 K.

2.1. Synthesis of Nb(V)-containing synthetic saponite clay

The synthetic saponite clay containing Nb(V) sites in structural tetrahedral positions of the inorganic framework was synthesized through hydrothermal method [62–64]. The starting synthesis gel had a molar composition of [SiO_2:MgO:Al_2O_3:Na_2O:Nb(OEt)$_5$:H_2O] 1:0.835:0.056:0.056:0.01:20 (Scheme S1), resulting in a final synthetic saponite clay with high cation-exchange capacity (CEC), equal to 80.8 $\pm$ 16.9 meq/100 g (Fig. S1) and the following formal composition: $(Na)_{0.81}Mg_6(OH)_4(Al_{0.81}Nb_{0.07}Si_{7.11})O_{20}\bullet nH_2O$, with n =

20.

Specifically, 0.13 mol of fumed SiO_2 was gradually dispersed in a solution consisting of 0.01 mol of NaOH in 50 mL of ultrapure water. The resulting gel was carefully mixed for 1 h. Then, 0.09 mol of $Mg(CH_3COO)_2 \bullet 4H_2O$ and 0.01 mol of Al(*i*-OPr)$_3$ were added to the gel and the mixture was stirred for further 2 h. Afterwards, 0.001 mol of liquid niobium ethoxide ($Nb(OEt)_5$, 99.95 %) was added and the gel was stirred for 15 min. The gel (with a pH between 8 and 9) was then introduced into a 125 mL Teflon cup in an autoclave (Anton Paar 4748) and heated at 513 K for 72 h. After the hydrothermal treatment, the product was rinsed with hot ultrapure water up to neutral pH and dried overnight at 373 K. The resulting material was named NbSAP. A corresponding Na^+-exchanged NbSAP clay (named Na-NbSAP) was also prepared to determine the cation-exchange capacity of the metal-functionalized saponite, following a procedure adapted from our previous studies [59,66,67]. Specifically, 2 g of NbSAP clay was dispersed in 200 mL of saturated sodium chloride solution (NaCl, ≥99.0 %) for 36 h at 298 K. This procedure ensures a proper chemical uniformity of the exchange sites of the clay, with a complete replacement of the cations within the interlamellar region (*i.e.* Al^{3+}, Mg^{2+}, H^+) by Na^+ only. The solid hence obtained, called Na-NbSAP, was then centrifuged with ultrapure water (7500 rpm for 5 min) until complete removal of chloride ions (confirmed by $AgNO_3$ spot test) and finally dried at 373 K overnight.

2.2. Synthesis of Na^+-exchange synthetic saponite clay

The synthetic saponite clay containing only Na^+ ions in the interlayer gallery was prepared following a procedure adapted from our previous studies [59,66,67].

2.3. Paraoxon-ethyl pesticide solution

2.3.1. Paraoxon-ethyl solution in anhydrous solvent at 550 ppm (2.00 mM)

250 mg of paraoxon-ethyl (diethyl *p*-nitrophenyl phosphate) was dissolved in 0.5 L of anhydrous solvent (ethyl acetate, AcOEt, or dichloromethane, DCM), stirred vigorously for a few minutes and then stored in a refrigerator at 277 K. Anhydrous solvent were obtained by storing them over 3A activated molecular sieve beads.

2.3.2. Paraoxon-ethyl solution at 200 ppm (0.73 mM)

100 mg of paraoxon-ethyl (diethyl *p*-nitrophenyl phosphate) was dissolved in 0.5 L of solvent (ultrapure water, anhydrous ethyl acetate or anhydrous dichloromethane), stirred vigorously for a few minutes and then stored in a refrigerator at 277 K.

2.4. Abatement tests

The experiments in anhydrous solvents were performed under very mild conditions at neutral pH, 298 K and 1 atm pressure. Specifically, 40 mg of solid catalyst (NbSAP, commercial Nb_2O_5 or Na-SAP) were taken as such, without any thermal pre-treatment, and added to 10 mL of paraoxon-ethyl solution in anhydrous solvent at 200 or 550 ppm in a batch glass reactor, previously purged with dry N_2 for 10 min, under continuous stirring. Experiments with no solids (blank tests) were also carried out using the same procedure. The distribution of the pesticide degradation reaction products was monitored by GC-FID analysis. Concentration profile graphs are expressed as relative concentration of paraoxon-ethyl with respect to its initial concentration at time zero.

The OP degradation reaction monitored in aqueous solution followed the same experimental conditions, using 10 mL of the paraoxon-ethyl aqueous solution at 200 ppm. The reaction was monitored by UV–Vis spectroscopy: 555 μL of each filtered liquid sample (supernatant), taken at different contact times, was diluted with 2485 μL of ultrapure water in a 3.0 mL quartz cuvette. A blank test (no solid) was also carried out using the same procedure.

All the above experiments were repeated three times for statistical purposes. The average experimental error was found to be 0.3 % for blank, 3.1 % for Nb_2O_5 and 1.9 % for NbSAP tests.

The reaction products in water over time was analysed by liquid-state ^{31}P NMR spectroscopy: 540 μL of each filtered liquid sample (taken at different contact times) + 60 μL of D_2O (10 % v/v; 99.9 atom % D) were placed in 5 mm NMR tubes.

^{31}P solid-state NMR spectroscopy was used to identify the products adsorbed on NbSAP after 24 h of reaction in water, while CHN analysis was employed to further assess the presence and to quantify the amount of organic species present on the solid surface. The spent solid was carefully rinsed with water and dried at 323 K overnight before analysis.

ICP-AES analysis of an aliquot of the solid-free liquid filtrate from the first catalytic cycle in water with NbSAP, mineralised in 70 % HNO_3 and 48 % HF prior the measure, revealed no measurable traces of niobium species leached into the reaction solution.

2.5. Regeneration tests

For the recycling tests, the spent NbSAP powder was carefully filtered, rinsed with plenty of ultrapure water and calcined under dry air at 773 K for 1 h (3 K/min) in a horizontal tube furnace [63]. The regenerated powder was cooled to room temperature *in vacuo* and then used for a second and third paraoxon-ethyl abatement run. Each catalytic run was repeated three times for statistical purposes.

2.6. Characterisation techniques

The cation exchange capacity (CEC) of the synthetic saponite clays was determined according to the standardised method based on

hexaaminecobalt trichloride solution and Ultraviolet–Visible (UV–Vis) spectrophotometry [68] (see Supporting *Information* for further details).

X-ray powder diffractograms (XRPD) were collected on unoriented ground powders on a Bruker D8 Advance Powder Diffractometer (Karlsruhe, Germany), operating in Bragg-Brentano geometry, with a Cu anode target equipped with a Ni filter (used as X-ray source) and with a Lynxeye XE-T high-resolution position-sensitive detector. The Trio and Twin/Twin optics are mounted on the DaVinci.Design modular XRD system. The X-ray tube of the instrument operates with a Cu-$K_{\alpha 1}$ monochromatic radiation ($\lambda = 1.54062$ Å), with the current intensity and the operating electric potential difference set to 40 mA and 40 kV, respectively, and with automatically variable primary divergent slits and primary and secondary Soller slits of 2.5°. Wide-angle X-ray profiles were recorded in the 5°–65° 2θ range at room temperature with a coupled 2θ-θ method, continuous PSD fast scan mode, time per step (rate or scan speed) of 0.100 s/step, and 2θ step size (increment) of 0.01°, with synchronization of the air scatter (or anti-scatter) knife and slits to automatic and with the fixed illumination sample set at 15 mm.

High-resolution transmission electron microscopy (HRTEM) micrographs were taken on a Zeiss Libra200 FE3010 High Resolution Transmission Electron Microscope (Munich, Germany) operating at 200 kV. NbSAP specimen was prepared by depositing the solid powder on a carbon-coated grid. The average $d_{(001)}$-spacing of the sample was determined via analysis of 100 lamellar distances on higher-magnification micrographs.

NbSAP clay was analysed by UV–Vis diffuse reflectance (UV–Vis DR) spectroscopy. The solid was dispersed in barium sulphate ($BaSO_4$, 99 %) at 20 wt% for the measurement. The spectrum was measured in air at room temperature in the 200–500 nm range with a resolution of 1 nm. For liquid-phase abatement tests with NbSAP and commercial Nb_2O_5, spectra of filtered liquid samples were measured at room temperature in the 230–600 nm range with a resolution of 1 nm. Liquid and solid phase spectra were recorded using a double-beam PerkinElmer Lambda 900 Spectrophotometer (Waltham, MA, USA).

In order to determine Nb content, elemental analysis was performed on an Ametek Spectro Genesis EOP Inductively Coupled Plasma Atomic Emission Spectrometer (ICP-AES) (Kleve, Germany) equipped with a cross-flow nebuliser, with simultaneous spectrum acquisition in the 175–770 nm wavelength range. NbSAP, and an aliquot of the filtered aqueous supernatant after 24 h of catalysis in the presence of the saponite, were mineralised in a mixture of HNO_3 70 % and HF 48 % at 373 K for 8 h. Then, the samples were opportunely diluted to 1 % w/v HNO_3 solutions before analysis.

N_2 physisorption measure of NbSAP was performed at 77 K in the relative pressure range from 10^{-6} to 1 P/P_0 by using a Quantachrome Autosorb 1MP/TCD instrument (Florida, USA). The saponite was outgassed at 523 K for 3 h. Specific surface area was determined using the multi-point Brunauer–Emmett–Teller (BET) equation, in the residual pressure range of 0.01–0.1 P/P_0. Pore size distribution was obtained using the non-local density functional theory (NLDFT) method.

Fourier transform infrared spectroscopy (FTIR) measurements were performed on a Thermo Electron Corporation FT Nicolet 5700 Spectrometer (Waltham, MA, USA), operating in the 4000–400 cm^{-1} range with a resolution of 4 cm^{-1}. Self-supporting pellets of each solid were placed in a special IR cell equipped with KBr windows, permanently connected to a vacuum line (residual pressure $<10^{-4}$ mbar). The experimental setup adopted allowed simple vacuum measurements, temperature treatments and ammonia adsorption-desorption experiments to be carried out *in situ*. Materials were first measured in vacuum at the infrared beam temperature (approx. 308 K). Prior to $NH_{3(g)}$ adsorption-desorption tests, samples were outgassed at 623 K with a heating ramp of 10 K/min for 3 h, using a special oil-free apparatus and a grease-free vacuum line to remove adsorbed water molecules from their surface. Samples were cooled down at room temperature prior to collecting spectra after $NH_{3(g)}$ adsorption at 50 mbar of gas. Spectra were normalised using the intensity of the overtones and combination modes of the saponite framework (bands in the 2200-1600 cm^{-1} range) as reference. In this way, differences in the intensity of bands across multiple samples related to intrinsic oscillators (*i.e.* hydroxyl groups) between different samples can be related to actual differences in the amount of such species in the materials. Due to the normalization, the absorbance values are reported in arbitrary units [a.u.].

Gas Chromatography (GC) was performed over an Agilent 6890 GC equipped with Flame-Ionization Detector (GC-FID) analysis (HP5, 30 m column; split mode).

One-dimensional (1D) heteronuclear ^{31}P nuclear magnetic resonance (NMR) spectra in solution were recorded at 300 K using a Bruker Advance III Spectrometer (Rheinstetten, Germany) equipped with a standard-bore 11.7 T magnet. The liquid samples taken from the experiments were prepared as described in Section 2.4. The ^{31}P NMR spectrum of paraoxon-ethyl alone was also recorded as a reference. The NMR spectrometer is equipped with a 5 mm double resonance Z-gradient broadband probe, with the inner coil optimized for observing nuclei between ^{31}P and ^{15}N and for ^{19}F and a Bruker BVT-3000 unit for temperature control. Chemical shifts are reported using the δ [ppm] scale and are externally referenced to tetramethylsilane (TMS) at 0 ppm.

Solid-state NMR (ssNMR) spectrum of NbSAP was acquired using a wide-bore, 11.74 T magnet and a Bruker Avance III 500 Spectrometer (Rheinstetten, Germany) equipped with a 4 mm triple resonance probe in double resonance mode. The operating frequencies for ^1H and ^{31}P were 500.13 and 202.46 MHz, respectively. The powder sample was packed in a zirconia rotor, sealed with a Kel-F cap and spun at a magic angle spinning (MAS) rate of 15 kHz at 300 K. ^{31}P MAS NMR spectrum was acquired with a 90° pulse and the magnitude of the radiofrequency field was 83 kHz with ^1H decoupling during acquisition. The spectrum was recorded using 8192 transients with a relaxation delay between accumulations of 30 s. Chemical shifts are reported using the δ scale and are externally referenced to ammonium dihydrogen phosphate at 0.8 ppm for ^{31}P.

CHN elemental analysis were performed using an EA3000 CHN Elemental Analyzer (EuroVector, Milan, Italy). Acetanilide, purchased from EuroVector (Milan, Italy), was used as calibration standard (C % = 71.089, H % = 6.711, N % = 10.363).

3. Results and discussion

3.1. Characterization of material

Synthetic saponite clay containing Nb(V) metal centres in tetrahedral positions of the inorganic framework was prepared by an optimized hydrothermal synthesis with a H_2O/Si ratio of 20 (Scheme S1) [62–64], resulting in a saponite with high cation-exchange capacity (CEC) of 80.8 ± 16.9 meq/100 g (Fig. S1). Nb(V) sites have been incorporated into the clay structure to make them more chemically stable and less susceptible to leaching during the abatement tests [63].

As revealed by XRD and TEM analysis, the material showed the typical structure and morphology of smectite clays, characterized by reflections indicative of a 2:1 T-O-T structure (Fig. S2), with an average 2D-lamella length of approx. 100 nm (Fig. S3) [59–61]. As already evidenced, the inclusion of Nb(V) did not alter the clay framework.

The content of Nb(V) species in the clay, evaluated by digestion of the solid and subsequent analysis by optical ICP instrument, was estimated to be 0.10 mmol/g, in line with parent sample [63]. These species are present in both tetrahedral (T_d) and octahedral (O_h) coordination states [69], as shown by two main bands at 235 nm (charge-transfer from $O^{2-} \rightarrow Nb^{5+}$ in T_d state) and 275 nm (structural O_h sites) in the UV–Vis Diffuse Reflectance spectrum (Fig. S4). Although a small amount of oligomers is present (320 nm) [62,70], no large extra-framework Nb_2O_5 were noticed [71].

NbSAP presents a IV-type textural isotherm with a H3 hysteresis loop, typical of mesoporosity due to non-ordered lamellae aggregates (Fig. S5A) [59,72]. The sample has a specific surface area of 335 m^2/g and exhibits a monomodal pore size distribution centred at 5.3 nm with pore volume of 0.450 cm^3/g (Fig. S5B). FTIR analysis of adsorbed $NH_{3(g)}$ at beam temperature was used to estimate the amount of Brønsted acid sites in the NbSAP clay (Fig. 1A-b), by integrating the band at 1450 cm^{-1} related to the δ_{as} NH_4^+ formed by interaction of NH_3 with the Si-O(H^+)-Al/–Nb sites (Fig. 1B) [73–75]. The acid sites density resulted to be 0.102 mmol/g, and this high value (for a synthetic clay) [76] was largely achieved thanks to the inclusion of Nb(V) species into structural positions of the

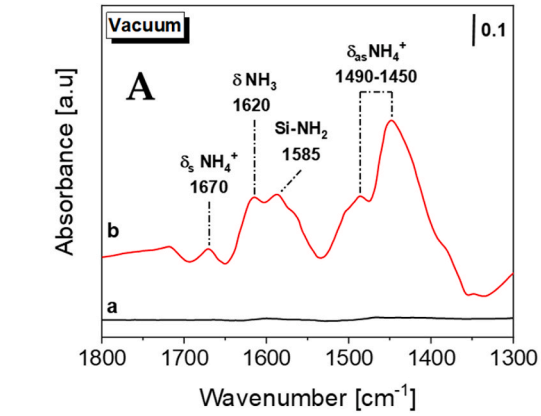

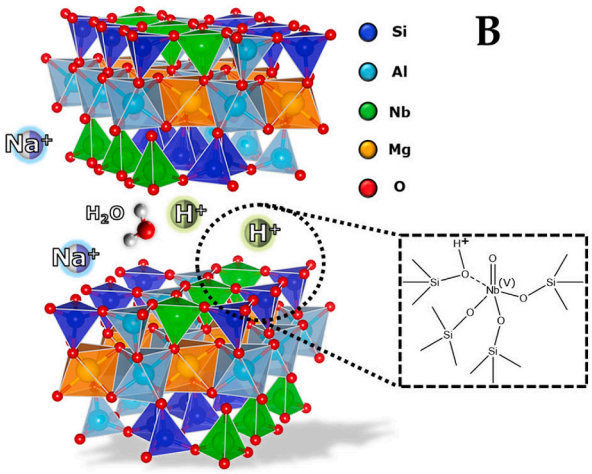

Fig. 1. (A) FTIR spectra of NH_3 (50 mbar) adsorbed and then evacuated at beam temperature for 90 min on commercial Nb_2O_5 (a) and synthetic NbSAP clay (b). Samples were previously outgassed at 623 K for 3 h prior the analysis; spectra are reported after subtraction of the bare samples. (B) Graphical representation of Na^+-related base sites and of a Brønsted acid site in NbSAP.

clay structure [62,64]. A commercial Nb_2O_5 sample (Fig. 1A–a), used for comparison, does not display any noteworthy Brønsted acidity (only 0.05 mmol/g).

3.2. Catalytic abatement tests of paraoxon-ethyl

The degradation of paraoxon-ethyl by synthetic NbSAP clay was tested under very mild reaction conditions (neutral pH, room temperature and ambient pressure). A concentration of 200 ppm (0.73 mM) of the pesticide in solution was used during the tests. The concentration of Nb(V) species and Brønsted acid sites in the amount of clay used in the catalytic runs resulted to be 0.400 mM and 0.408 mM, respectively. Blank tests in the absence of solid catalysts were carried out as a reference. To evaluate the role of Nb(V) sites in a benchmark oxidic matrix, the performance of the Nb-containing saponite clay was compared to the one of commercial Nb_2O_5 as well as of a saponite with no Nb centres (Fig. S6).

Chlorinated solvents are ideal media for OPPs, although they are not environmentally sustainable. So, only for a preliminary study of the degradation of paraoxon-ethyl in organic solvent, the reaction was first studied in anhydrous dichloromethane (DCM) and monitored along 24 h (Fig. 2 and S7). In the presence of NbSAP, the concentration of paraoxon-ethyl decreased by 30 % after the first hour and by 53 % after 24 h (Fig. 2). In comparison, only a reduction of approx. 6 % was observed with Nb_2O_5 after 24 h (Fig. 2). These results first highlight the importance of the acid site density in the catalytic degradation of paraoxon-ethyl in DCM solvent. NbSAP was able to degrade a large amount of the organophosphorus substrate in the organic medium by exploiting the added strength of Brønsted acid sites caused by the insertion of Nb centres in the clay structure [62,64]. This effect was not observed in the presence of Nb_2O_5, as it does not possess significant Brønsted acidity.

At the same time, a non-negligible contribution to paraoxon degradation is to be attributed to the Na^+-containing fraction of saponite support too. In fact, when a fully exchanged sample of saponite clay with no Nb in the framework is used as a catalyst (Na-SAP in Fig. S6), a noteworthy diminution of OP concentration was recorded. In the first hour of reaction, the paraoxon-ethyl was degraded, even more rapidly than over NbSAP. Later, however, the degradation process slowed down and barely 40 % of the initial OP was degraded for longer reaction times. Such degradation capability is likely due to the alkaline hydrolysis of paraoxon promoted by the moderately basic character of fully Na^+-exchanged smectite clays. These sites are generated upon Na^+ exchange and have shown to be able to carry out base-catalysed transformations, such as transesterification or Knoevenagel condensation reactions [77–79].

In the case of NbSAP, the two hydrolytic capabilities are synergistically merged: the acid sites due to Nb(V) centres within the TOT clay framework and the basic character brought by the partial presence of Na^+ in the saponite structure, introduced along with the pristine synthesis gel (*v.* section 2.1). In this case, hydrolysis is likely carried out by small amounts of H_2O that are present as physisorbed water onto/into the clay and by -OH moieties on the edge of the TOT layers of the clay (*cf.* Fig. 7 in ref. [77]).

The reaction was further studied in anhydrous ethyl acetate (AcOEt), a more sustainable polar aprotic solvent than DCM, and then in water, the most sought-after reaction medium. Over NbSAP, the performance was better than the one observed in DCM. Although the initial activity was similar, with 26 % conversion after 1 h, a gradual increase in the substrate conversion was recorded up to 87 % after 24 h (Fig. 2). Negligible conversion values were observed over the reference materials Nb_2O_5. In aqueous solution, the reaction was followed by UV–Vis spectroscopy, by monitoring the main absorption band of the organophosphorus pesticide at λ_{max} of 275 nm (Fig. S8) [80]. With no catalyst, the concentration of paraoxon-ethyl remained constant in water throughout the test and over Nb_2O_5 no significant activity was observed (approx. 3 % after 24 h) (Fig. 2). On the contrary, the presence of NbSAP caused a rapid decrease of the concentration of paraoxon-ethyl in water after the first hour (82 % conversion). Then, from 1 to 24 h, the substrate content remained essentially constant, with an overall conversion of 84 %. The catalytic performance of NbSAP was not affected by metal

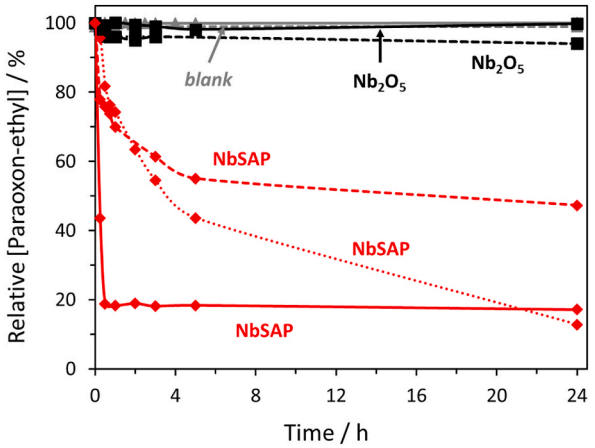

Fig. 2. Concentration profiles of paraoxon-ethyl in anhydrous DCM (dashed curves), in anhydrous AcOEt (dotted curves) and in H_2O (solid curves). Blank tests (▲, grey), tests over reference Nb_2O_5 (■, black) and over NbSAP (◆, red) are reported in the graph. Reaction conditions: 10 mL of 200 ppm (0.73 mM) paraoxon-ethyl solution, neutral pH, 298 K, 1 atm and 40 mg catalyst. (For interpretation of the references to colour in this figure legend, the reader is referred to the Web version of this article.)

leaching into solution, as no Nb(V) species were detected by ICP-AES analysis on the liquid filtrate after 24 h. The far higher catalytic activity of NbSAP observed in water with respect to the one recorded in organic solvents (DCM and AcOEt), is related to a better accessibility of the clay acid sites towards the substrate in aqueous solution. This is attributed to swelling phenomena of the saponite in water [81–83], whereas dichloromethane and ethyl acetate behave as non-swelling media [84,85] and to the hydrophobic character of the pesticide, which is less likely to dissolve in water than AcOEt and DCM. Moreover, NbSAP tends to settle down to the bottom of the vial after a few moments in DCM (Figs. S9 and a), whereas, in water, the formation of a homogeneous suspension, stable over time even without stirring, is clearly visible (Figs. S9 and b). This behaviour confirms the tendency of NbSAP to swell (and probably exfoliate) in

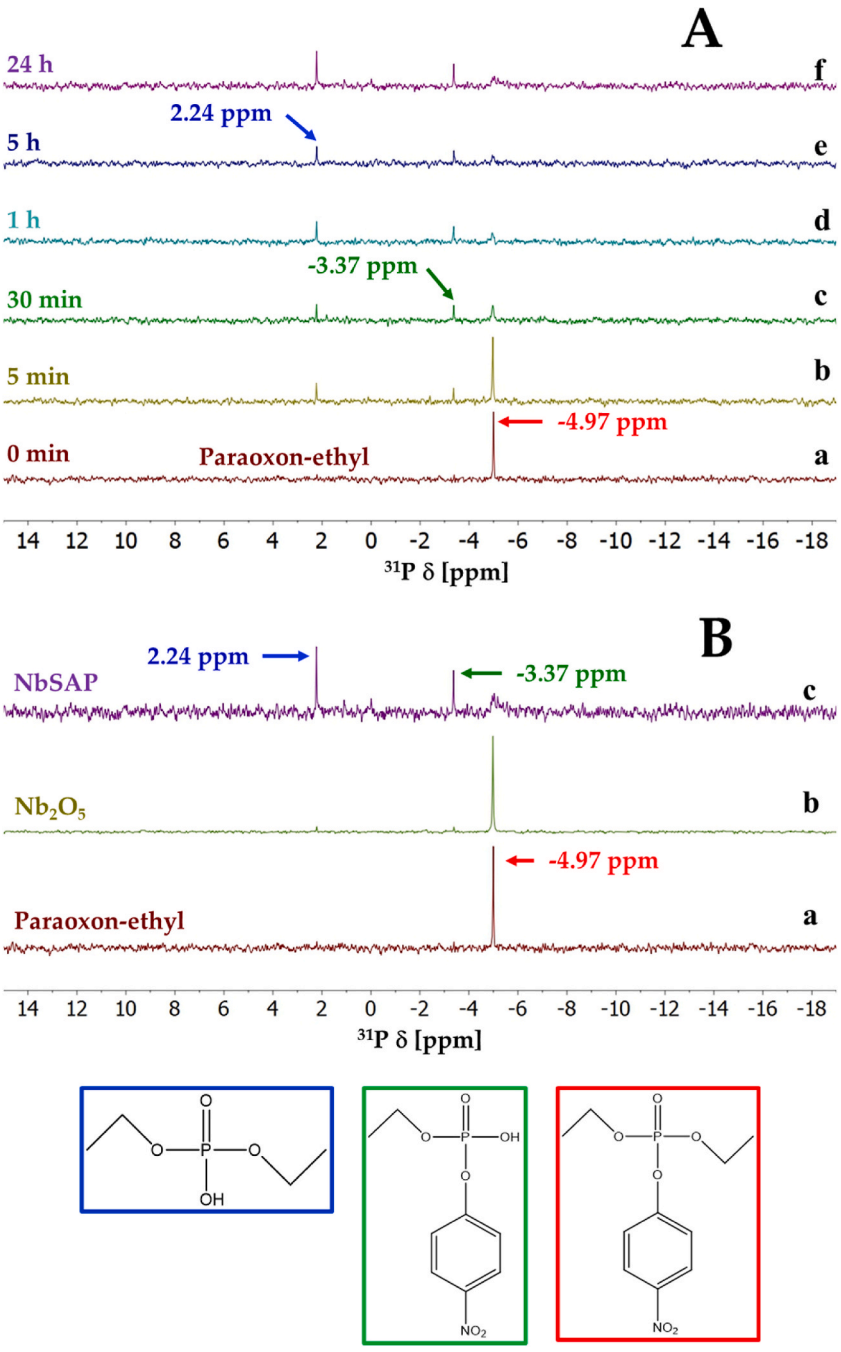

Fig. 3. (A) ^{31}P NMR spectra in water + D_2O (10 %) over time of paraoxon-ethyl treated with NbSAP. (B) ^{31}P NMR spectra in water + D_2O (10 %) of paraoxon-ethyl alone (a) and treated with commercial Nb_2O_5 (b) and NbSAP clay (c), after 24 h of reaction. The signals associated with paraoxon-ethyl (−4.97 ppm, red), ethyl-4-nitrophenyl hydrogen phosphate (−3.37 ppm, green) and diethyl phosphate (2.24 p.m., blue) species are reported in the figures. (For interpretation of the references to colour in this figure legend, the reader is referred to the Web version of this article.)

water, which leads to a better accessibility of its active reaction sites. Furthermore, in water, which is a worse solvent for paraoxon-ethyl than DCM or AcOEt, the quick adsorption of the pesticide on the clay structure is favoured since the first moments of the reaction and this leads to a very rapid disappearance of the substrate from the solution, even during the first hour of reaction.

In the UV–Vis spectra reported in Fig. S8D, it is possible to observe the appearance of a broad band with a λ_{max} at 400 nm, which becomes slightly more intense over time. This signal is due to the formation of 4-nitrophenol from the P-O-C cleavage reaction of paraoxon-ethyl [25,32,46,86], confirming the degradation of the organophosphorus agent in water and the role of NbSAP, which promotes the acid-mediated hydrolysis of the pesticide. Besides, no trace of 4-nitrophenol product was detected in the UV–Vis spectra when the pesticide was treated over Nb_2O_5 (Fig. S8C).

More information on the chemical nature of the degradation products of paraoxon-ethyl in water has been determined by high resolution ^{31}P NMR spectroscopy. Spectra were measured on solid-free aqueous samples spiked with 10 % of D_2O, taken at different contact times for NbSAP (Fig. 3A), and after 24 h of contact for Nb_2O_5 (Fig. 3B–b). The spectrum of paraoxon-ethyl in water is also reported in the figures as reference, with its signal located at −4.97 ppm [25]. Over NbSAP (Fig. 3A), a gradual decrease in intensity of the pesticide signal was observed from 5 min to 24 h, followed by the appearance of two new signals at −3.37 and 2.24 ppm assigned to ethyl 4-nitrophenyl hydrogen phosphate and diethyl phosphate species [25,32,45,46,86–88], with the latter representing one of the end-products of the acid-catalysed hydrolytic degradation process. The presence of diethyl phosphate is also compatible with the observation of 4-nitrophenol species in the relative UV–Vis spectra (Fig. S8D), as both compounds are formed by the cleavage reaction of the P-O-C bond in the paraoxon-ethyl molecule [25,32,45,46,86]. After 24 h, the paraoxon-ethyl peak almost completely disappeared, whereas the signals of the two main degradation products increased (Fig. 3B and c). In agreement with previous results, the use of Nb_2O_5 did not result in any significant conversion of paraoxon-ethyl in water.

The presence of adsorbed species on the surface of NbSAP was assessed using solid state ^{31}P MAS NMR spectroscopy, analysing the solid powder after 24 h of reaction in aqueous solution. This showed a very broad band in the 10 to −30 ppm range, in which contributions at −0.50 and −8.77 ppm were visible, as derived from the deconvolution of the main band (Fig. 4). These signals were assigned to phosphoric acid and paraoxon-ethyl adsorbed on the solid surface of NbSAP respectively [89,90], in a relative percentage ratio of 41:59 % (1:1.44 ratio) calculated from their integrated areas. The presence of phosphoric acid can be attributed to its high affinity to be adsorbed onto the solid due to its highly polar character. Paraoxon-ethyl was quantified by CHN elemental analysis as 0.008 ± 0.002 mmol/g (0.32 μmol per 40 mg of saponite catalyst used during tests), which is equal to 4.21 % of the initial amount of the organophosphorus pesticide in the volume of aqueous solution used (7.3 μmol). From this value, it was possible to estimate an amount of 5.5 μmol/g of phosphoric acid adsorbed on the spent NbSAP catalyst.

The results allow us to define that: *i*) a small fraction of the undegraded pesticide was removed from water by NbSAP through mere adsorption processes, and *ii*) the catalytically active acid sites due to Nb(V) centres, along with the basic character of the saponite support due to the partial presence of Na^+ ions, give rise to hydrolytic reactions able to lead to the almost total degradation of paraoxon.

The use of NbSAP catalyst led to a progressive conversion of paraoxon-ethyl in aqueous solution into ethyl-4-nitrophenyl hydrogen phosphate, 4-nitrophenol, diethyl phosphate and phosphoric acid. UV–Vis data showed that only 16 % of the initial content of the pesticide remains unchanged in solution, while the 84 %, which is no longer present, undergoes two main pathways: 1) approx. 4 % is

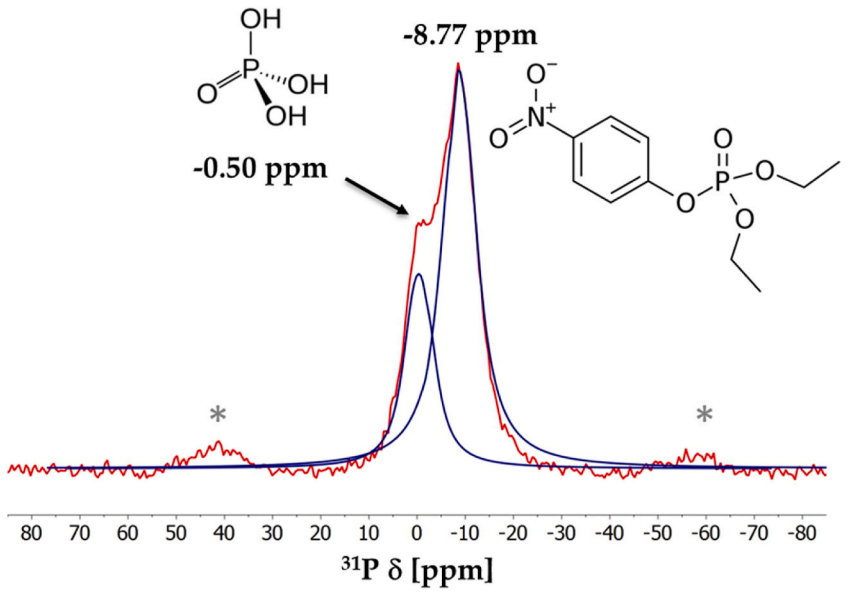

Fig. 4. Solid-state ^{31}P MAS NMR spectrum of spent NbSAP after 24 h of reaction in the paraoxon-ethyl aqueous solution at 200 ppm (0.73 mM). The deconvolution of the band is represented by blue curves. * denote spinning sidebands. (For interpretation of the references to colour in this figure legend, the reader is referred to the Web version of this article.)

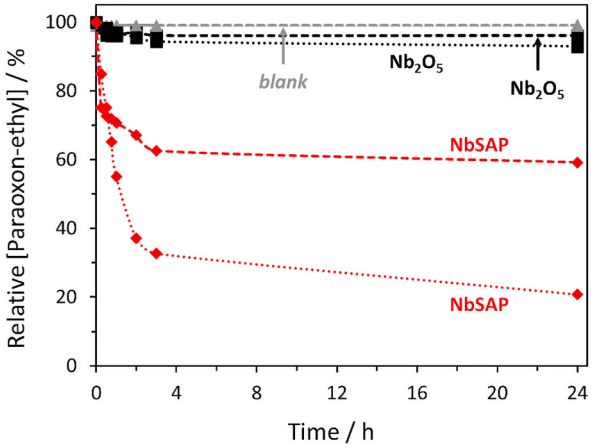

Fig. 5. Concentration profiles of paraoxon-ethyl in anhydrous DCM (dashed curves) and anhydrous AcOEt (dotted curves). Blank tests (▲, grey), tests over reference Nb_2O_5 (■, black) and over NbSAP (◆, red). Reaction conditions: 10 mL of paraoxon-ethyl solution in anhydrous AcOEt or DCM at 550 ppm (2.00 mM), neutral pH, 298 K, 1 atm and 40 mg catalyst. (For interpretation of the references to colour in this figure legend, the reader is referred to the Web version of this article.)

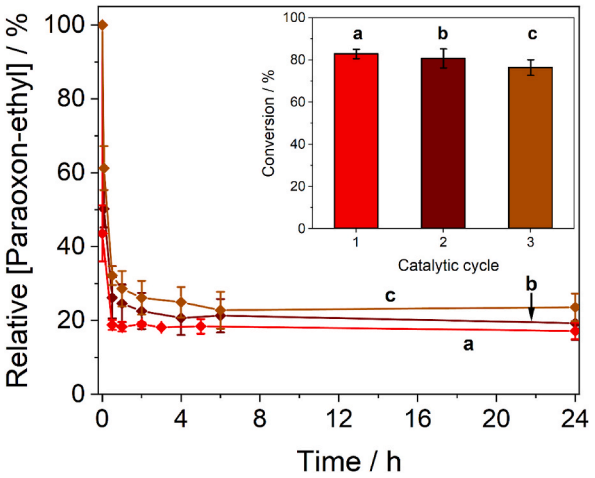

Fig. 6. Concentration profiles of paraoxon-ethyl aqueous solution in multiple degradation tests over NbSAP, for the first (a), second (b) and third (c) catalytic run. Reaction conditions: 10 mL of 200 ppm (0.73 mM) paraoxon-ethyl solution, neutral pH, 298 K, 1 atm and 40 mg catalyst. The spent solid was filtered, rinsed with ultrapure water and calcined 773 K (dry air) before the 2nd and 3rd cycles. The inset shows the paraoxon-ethyl conversion after 24 h.

adsorbed on the solid surface of NbSAP; 2) approx. 80 % of the remaining fraction is converted into the aforementioned degradation products. Among them, only the phosphoric acid has been detected on the solid, while the rest was present in the aqueous phase. The hydrolytic properties of NbSAP clay, together with increased accessibility of these acid sites in water, was able to promote a remarkable pesticide abatement activity. In the absence of these hydrolytic active sites, the commercial sample of Nb_2O_5 showed no catalytic activity in either medium.

Finally, aiming at mimicking the treatment of real-life heavily contaminated water streams and maximising the degradation capability, the NbSAP catalyst was tested on solutions with higher concentrations of paraoxon, up to 550 ppm (2.0 mM) (Fig. 5). The tests were performed in organic DCM and AcOEt only, as paraoxon-ethyl is no longer soluble in water at this concentration (and no homogeneous reaction solution of the pesticide can thus be obtained). AcOEt was the solvent where the highest values of pesticide conversion were attained: 45 % after 1 h and approx. 80 % after 24 h of reaction time. Poorer performances were observed in DCM, instead, where a maximum conversion of 41 % was reached after 24 h. The reference Nb_2O_5 catalyst proved to be virtually inactive in both solvents under these conditions. AcOEt can therefore be a suitable medium for the liquid-phase safe abatement of stockpiled amounts of obsolete organophosphorus agrochemicals, considering that higher concentrations of paraoxon-ethyl can be obtained in AcOEt than in aqueous solutions.

3.3. Regeneration tests of NbSAP material

The possibility to regenerate the saponite clay for further pesticide degradation runs was investigated. The spent NbSAP was filtered, rinsed with abundant water and calcined under dry air at high temperature to remove the adsorbed organic content [63]. The performance of regenerated NbSAP was studied in two further paraoxon-ethyl abatement runs. The sample kept its catalytic properties well over three cycles, with only minor performance fluctuations in the early hours of the second and third runs, likely due to organic compound accumulation on the solid's surface, which could hinder pesticide molecule access to NbSAP reaction sites (Table S1). The degradation of paraoxon-ethyl in aqueous phase reached 80 % in the second cycle (Fig. 6, curve b) and 77 % in the third cycle (Fig. 6, curve c), closely matching the 84 % observed in the first cycle (Fig. 6, curve a). These results highlight the robustness of NbSAP in multiple tests too.

4. Conclusions

This study investigates the use of a Nb(V)-containing synthetic saponite clay for the degradation of the anti-cholinergic pesticide paraoxon-ethyl under environmentally friendly conditions. The peculiar nature of this heterogeneous catalyst allowed us to exploit the multifunctional character of the solid, with both adsorption and hydrolytic capabilities, without adding external co-reactants to the reaction medium. The clay was prepared through one-pot hydrothermal procedure, resulting in a solid featuring an optimal synergistic mix of strong surface Brønsted acidity and moderate basic hydrolytic capability. The synthetic Nb-containing saponite demonstrated good performance in terms of degradation of the organophosphorus agrochemical in water and in ethyl acetate as solvents. More than 80 % of the initial concentration of paraoxon-ethyl was converted into non-noxious products in both media, thanks to a cooperative adsorption, acid-catalysed degradation and alkaline hydrolysis of the substrate. Such promising activity is due to the presence of remarkable density and strength of acid sites (with respect to the average for a synthetic clay) obtained through the tailored inclusion of Nb(V) species in structural positions of the solid framework. The co-presence of Na^+, introduced with the pristine synthesis gel at the exchangeable sites of the clay, enhances the hydrolytic capability of the solid. Moreover, in aqueous phase, the accessibility by substrate molecules towards the acid sites of NbSAP is made easier by the combined swelling phenomena of the lamellae and the marked hydrophilic/hydrophobic affinity of the clay with paraoxon-ethyl. NbSAP showed excellent regeneration and reuse capability, retaining its ability to degrade the organophosphorus agent in water after three cycles.

In conclusion, the synthetic Nb(V)-saponite clay investigated in this study is a potential candidate not only for the safe, mild and sustainable degradation of toxic organophosphorus agrochemicals in aqueous phase, but also for the decontamination of highly hazardous anti-cholinergic compounds, among which the internationally banned nerve chemical warfare agents.

CRediT authorship contribution statement

Stefano Marchesi: Writing – review & editing, Writing – original draft, Methodology, Investigation, Formal analysis, Data curation, Conceptualization. **Stefano Econdi:** Writing – review & editing, Methodology, Investigation, Formal analysis, Data curation, Conceptualization. **Geo Paul:** Writing – review & editing, Formal analysis, Data curation. **Fabio Carniato:** Writing – review & editing, Supervision, Methodology, Data curation, Conceptualization. **Leonardo Marchese:** Writing – review & editing. **Matteo Guidotti:** Writing – review & editing, Supervision, Methodology, Data curation, Conceptualization. **Chiara Bisio:** Writing – review & editing, Supervision, Methodology, Data curation, Conceptualization.

Data and code availability

Data will be made available on request.

Declaration of competing interest

The authors declare that they have no known competing financial interests or personal relationships that could have appeared to influence the work reported in this paper.

Acknowledgements

The authors would like to thank Elena Perin (DiSIT, Università del Piemonte Orientale, Alessandria, Italy) for the CHN analysis. The authors would like to thank the SCITEC PerBiocid project [project@CNR 2020: SAC.AD002.173.032] for the funding provided.

Appendix B. Supplementary data

Supplementary data to this article can be found online at https://doi.org/10.1016/j.heliyon.2024.e39898.

References

[1] K.L.G. Farizatto, B.A. Bahr, Paraoxon: an anticholinesterase that triggers an excitotoxic cascade of oxidative stress, adhesion responses, and synaptic compromise, Eur. Sci. J. 13 (2017) 29–37, https://doi.org/10.19044/esj.2017.c1p4.

[2] N. Tabassum, U. Rafique, K.S. Balkhair, M.A. Ashraf, Chemodynamics of methyl parathion and ethyl parathion: adsorption models for sustainable agriculture, BioMed Res. Int. 2014 (2014) e831989, https://doi.org/10.1155/2014/831989.

[3] D. Mohapatra, S.K. Rath, P.K. Mohapatra, Accelerated degradation of four organophosphorus insecticides by malathion tolerant Aspergillus Niger MRU01 a soil fungus, Geomicrobiol. J. 0 (2023) 1–10, https://doi.org/10.1080/01490451.2023.2259912.

[4] M. Kushwaha, S. Verma, S. Chatterjee, Profenofos, an acetylcholinesterase-inhibiting organophosphorus pesticide: a short review of its usage, toxicity, and biodegradation, J. Environ. Qual. 45 (2016) 1478–1489, https://doi.org/10.2134/jeq2016.03.0100.

[5] A.O. Affum, S.O. Acquaah, S.D. Osae, E.E. Kwaansa-Ansah, Distribution and risk assessment of banned and other current-use pesticides in surface and groundwaters consumed in an agricultural catchment dominated by cocoa crops in the Ankobra Basin, Ghana, Sci. Total Environ. 633 (2018) 630–640, https://doi.org/10.1016/j.scitotenv.2018.03.129.

[6] G. Manco, E. Porzio, Y. Suzumoto, Enzymatic detoxification: a sustainable means of degrading toxic organophosphate pesticides and chemical warfare nerve agents, J. Chem. Technol. Biotechnol. 93 (2018) 2064–2082, https://doi.org/10.1002/jctb.5603.

[7] Y. Liu, F. Liu, X. Pan, J. Li, Protecting the environment and public health from pesticides, Environ. Sci. Technol. 46 (2012) 5658–5659, https://doi.org/10.1021/es301652v.

[8] B.P. Shah, B. Devkota, Obsolete pesticides: their environmental and human health hazards, Journal of Agriculture and Environment 10 (2009) 60–66, https://doi.org/10.3126/aej.v10i0.2130.

[9] I. Katsikantami, C. Colosio, A. Alegakis, M.N. Tzatzarakis, E. Vakonaki, A.K. Rizos, D.A. Sarigiannis, A.M. Tsatsakis, Estimation of daily intake and risk assessment of organophosphorus pesticides based on biomonitoring data – the internal exposure approach, Food Chem. Toxicol. 123 (2019) 57–71, https://doi.org/10.1016/j.fct.2018.10.047.

[10] I. Hertz-Picciotto, J.B. Sass, S. Engel, D.H. Bennett, A. Bradman, B. Eskenazi, B. Lanphear, R. Whyatt, Organophosphate exposures during pregnancy and child neurodevelopment: recommendations for essential policy reforms, PLoS Med. 15 (2018) e1002671, https://doi.org/10.1371/journal.pmed.1002671.

[11] C. Dereumeaux, C. Fillol, P. Quenel, S. Denys, Pesticide exposures for residents living close to agricultural lands: a review, Environ. Int. 134 (2020) 105210, https://doi.org/10.1016/j.envint.2019.105210.

[12] D.J. Angelini, R.A. Moyer, S. Cole, K.L. Willis, J. Oyler, R.M. Dorsey, H. Salem, The pesticide metabolites paraoxon and malaoxon induce cellular death by different mechanisms in cultured human pulmonary cells, Int. J. Toxicol. 34 (2015) 433–441, https://doi.org/10.1177/1091581815593933.

[13] M. Guidotti, F. Trifirò, Chemical risk and chemical warfare agents: science and technology against humankind, Toxicol. Environ. Chem. 98 (2016) 1018–1025, https://doi.org/10.1080/02772248.2014.996153.

[14] A. Elbouzidi, M. Addi, Chapter 18 - chemical warfare: unprecedented environmental threat, in: S. Das, S. Thomas, P.P. Das (Eds.), Sensing of Deadly Toxic Chemical Warfare Agents, Nerve Agent Simulants, and Their Toxicological Aspects, Elsevier, 2023, pp. 423–429, https://doi.org/10.1016/B978-0-323-90553-4.00021-4.

[15] J. Kaushal, M. Khatri, S.K. Arya, A treatise on Organophosphate pesticide pollution: current strategies and advancements in their environmental degradation and elimination, Ecotoxicol. Environ. Saf. 207 (2021) 111483, https://doi.org/10.1016/j.ecoenv.2020.111483.

[16] K. Kim, O.G. Tsay, D.A. Atwood, D.G. Churchill, Destruction and detection of chemical warfare agents, Chem. Rev. 111 (2011) 5345–5403, https://doi.org/10.1021/cr100193y.

[17] K. Bano, S. Kaushal, P.P. Singh, A review on photocatalytic degradation of hazardous pesticides using heterojunctions, Polyhedron 209 (2021) 115465, https://doi.org/10.1016/j.poly.2021.115465.

[18] M. Hadei, A. Mesdaghinia, R. Nabizadeh, A.H. Mahvi, S. Rabbani, K. Naddafi, A comprehensive systematic review of photocatalytic degradation of pesticides using nano TiO2, Environ. Sci. Pollut. Res. 28 (2021) 13055–13071, https://doi.org/10.1007/s11356-021-12576-8.

[19] S.O. Pehkonen, Q. Zhang, The degradation of organophosphorus pesticides in natural waters: a critical review, Crit. Rev. Environ. Sci. Technol. 32 (2002) 17–72, https://doi.org/10.1080/10643380290813444.

[20] V.B. Silva, Y.H. Santos, R. Hellinger, S. Mansour, A. Delaune, J. Legros, S. Zinoviev, E.S. Nogueira, E.S. Orth, Organophosphorus chemical security from a peaceful perspective: sustainable practices in its synthesis, decontamination and detection, Green Chem. 24 (2022) 585–613, https://doi.org/10.1039/D1GC02705K.

[21] S. Mansour, V.B. Silva, E.S. Orth, J. Legros, Soft detoxification of chemical warfare agent simulants and pesticides under pressure, Org. Biomol. Chem. 20 (2022) 7604–7608, https://doi.org/10.1039/D2OB01217K.

[22] J.G.L. Ferreira, W.H. Takarada, E.S. Orth, Waste-derived biocatalysts for pesticide degradation, J. Hazard Mater. 427 (2022) 127885, https://doi.org/10.1016/j.jhazmat.2021.127885.

[23] V.B. Silva, L.L.Q. Nascimento, M.C. Nunes, R.B. Campos, A.R.M. Oliveira, E.S. Orth, Puzzling reaction of imidazole with methyl parathion: P=S versus P=O mechanistic shift dilemma in organophosphates, Chem. Eur J. 25 (2019) 817–822, https://doi.org/10.1002/chem.201804107.

[24] R.B. Campos, V.B. Silva, L.R.A. Menezes, F.M.M. Ocampos, J.M. Fernandes, A. Barison, A.R.M. Oliveira, D.J. Tantillo, E.S. Orth, Competitive reactivity of tautomers in the degradation of organophosphates by imidazole derivatives, Chem. Eur J. 26 (2020) 5017–5026, https://doi.org/10.1002/chem.201905379.

[25] P. Pavez, D. Millán, J.I. Morales, E.A. Castro, C. López A, J.G. Santos, Mechanisms of degradation of paraoxon in different ionic liquids, J. Org. Chem. 78 (2013) 9670–9676, https://doi.org/10.1021/jo401351v.

[26] I.V. Borkar, C.Z. Dinu, G. Zhu, R.S. Kane, J.S. Dordick, Bionanoconjugate-based composites for decontamination of nerve agents, Biotechnol. Prog. 26 (2010) 1622–1628, https://doi.org/10.1002/btpr.498.

[27] H.D. Lu, I.R. Wheeldon, S. Banta, Catalytic biomaterials: engineering organophosphate hydrolase to form self-assembling enzymatic hydrogels, Protein Eng. Des. Sel. 23 (2010) 559–566, https://doi.org/10.1093/protein/gzq026.

[28] L. Zhao, C. Deng, S. Xue, H. Liu, L. Hao, M. Zhu, Multifunctional g-C3N4/Ag NPs intercalated GO composite membrane for SERS detection and photocatalytic degradation of paraoxon-ethyl, Chem. Eng. J. 402 (2020) 126223, https://doi.org/10.1016/j.cej.2020.126223.

[29] M.A. Astle, G.A. Rance, M.W. Fay, S. Notman, M.R. Sambrook, A.N. Khlobystov, Synthesis of hydroxylated group IV metal oxides inside hollow graphitised carbon nanofibers: nano-sponges and nanoreactors for enhanced decontamination of organophosphates, J. Mater. Chem. A 6 (2018) 20444–20453, https://doi.org/10.1039/C8TA08100J.

[30] S.F. Blaskievicz, W.G. Endo, A.J.G. Zarbin, E.S. Orth, Magnetic nanocatalysts derived from carbon nanotubes functionalized with imidazole: towards pesticide degradation, Appl. Catal. B Environ. 264 (2020) 118496, https://doi.org/10.1016/j.apcatb.2019.118496.

[31] I. Trenque, G.C. Magnano, M.A. Bolzinger, L. Roiban, F. Chaput, I. Pitault, S. Briançon, T. Devers, K. Masenelli-Varlot, M. Bugnet, D. Amans, Shape-selective synthesis of nanoceria for degradation of paraoxon as a chemical warfare simulant, Phys. Chem. Chem. Phys. 21 (2019) 5455.

[32] G.K. Prasad, P.V.R.K. Ramacharyulu, J.P. Kumar, A.R. Srivastava, B. Singh, Photocatalytic degradation of paraoxon-ethyl in aqueous solution using titania nanoparticulate film, Thin Solid Films 520 (2012) 5597–5601, https://doi.org/10.1016/j.tsf.2012.04.033.

[33] J. Li, V.V. Singh, S. Sattayasamitsathit, J. Orozco, K. Kaufmann, R. Dong, W. Gao, B. Jurado-Sanchez, Y. Fedorak, J. Wang, Water-driven micromotors for rapid photocatalytic degradation of biological and chemical warfare agents, ACS Nano 8 (2014) 11118–11125, https://doi.org/10.1021/nn505029k.

[34] M. Sheydaei, M. Karimi, V. Vatanpour, Continuous flow photoelectrocatalysis/reverse osmosis hybrid reactor for degradation of a pesticide using nano N-TiO2/Ag/Ti electrode under visible light, J. Photochem. Photobiol. Chem. 384 (2019) 112068, https://doi.org/10.1016/j.jphotochem.2019.112068.

[35] T.G. Grissom, A.M. Plonka, C.H. Sharp, A.M. Ebrahim, Y. Tian, D.L. Collins-Wildman, A.L. Kaledin, H.J. Siegal, D. Troya, C.L. Hill, A.I. Frenkel, D.G. Musaev, W. O. Gordon, C.J. Karwacki, M.B. Mitchell, J.R. Morris, Metal–organic framework- and polyoxometalate-based sorbents for the uptake and destruction of chemical warfare agents, ACS Appl. Mater. Interfaces 12 (2020) 14641–14661, https://doi.org/10.1021/acsami.9b20833.

[36] Y. Hou, H. An, Y. Zhang, T. Hu, W. Yang, S. Chang, Rapid destruction of two types of chemical warfare agent simulants by hybrid polyoxomolybdates modified by carboxylic acid ligands, ACS Catal. 8 (2018) 6062–6069, https://doi.org/10.1021/acscatal.8b00972.

[37] Y. Liu, A.J. Howarth, N.A. Vermeulen, S.-Y. Moon, J.T. Hupp, O.K. Farha, Catalytic degradation of chemical warfare agents and their simulants by metal-organic frameworks, Coord. Chem. Rev. 346 (2017) 101–111, https://doi.org/10.1016/j.ccr.2016.11.008.

[38] T. Islamoglu, Z. Chen, M.C. Wasson, C.T. Buru, K.O. Kirlikovali, U. Afrin, M.R. Mian, O.K. Farha, Metal–organic frameworks against toxic chemicals, Chem. Rev. 120 (2020) 8130–8160, https://doi.org/10.1021/acs.chemrev.9b00828.

[39] W. Guo, H. Lv, K.P. Sullivan, W.O. Gordon, A. Balboa, G.W. Wagner, D.G. Musaev, J. Bacsa, C.L. Hill, Broad-spectrum liquid- and gas-phase decontamination of chemical warfare agents by one-dimensional heteropolyniobates, Angew. Chem. 128 (2016) 7529–7533, https://doi.org/10.1002/ange.201601620.

[40] L. Bromberg, H. Schreuder-Gibson, W.R. Creasy, D.J. McGarvey, R.A. Fry, T.A. Hatton, Degradation of chemical warfare agents by reactive polymers, Ind. Eng. Chem. Res. 48 (2009) 1650–1659, https://doi.org/10.1021/ie801150y.

[41] L.A. Giusti, M. Medeiros, N.L. Ferreira, J.R. Mora, H.D. Fiedler, Polymers containing imidazole groups as nanoreactors for hydrolysis of esters, J. Phys. Org. Chem. 27 (2014) 297–302, https://doi.org/10.1002/poc.3263.

[42] L. Bromberg, W.R. Creasy, D.J. McGarvey, E. Wilusz, T.A. Hatton, Nucleophilic polymers and gels in hydrolytic degradation of chemical warfare agents, ACS Appl. Mater. Interfaces 7 (2015) 22001–22011, https://doi.org/10.1021/acsami.5b06905.

[43] M. Malakootian, A. Shahesmaeili, M. Faraji, H. Amiri, S. Silva Martinez, Advanced oxidation processes for the removal of organophosphorus pesticides in aqueous matrices: a systematic review and meta-analysis, Process Saf. Environ. Protect. 134 (2020) 292–307, https://doi.org/10.1016/j.psep.2019.12.004.

[44] J.G.L. Ferreira, E.S. Orth, Amidoxime-derived rice husk as biocatalyst and scavenger for organophosphate neutralization and removal, Environ. Pollut. 330 (2023) 121802, https://doi.org/10.1016/j.envpol.2023.121802.

[45] V.A. Okello, I.O. K'Owino, K. Masika, V.O. Shikuku, Reduction and degradation of paraoxon in water using zero-valent iron nanoparticles, Sustainability 14 (2022) 9451, https://doi.org/10.3390/su14159451.

[46] S. Wang, L. Bromberg, H. Schreuder-Gibson, T.A. Hatton, Organophophorous ester degradation by chromium(III) terephthalate metal–organic framework (MIL-101) chelated to *N* , *N* -dimethylaminopyridine and related aminopyridines, ACS Appl. Mater. Interfaces 5 (2013) 1269–1278, https://doi.org/10.1021/am302359b.

[47] M. Movsisyan, E.I.P. Delbeke, J.K.E.T. Berton, C. Battilocchio, S.V. Ley, C.V. Stevens, Taming hazardous chemistry by continuous flow technology, Chem. Soc. Rev. 45 (2016) 4892–4928, https://doi.org/10.1039/C5CS00902B.

[48] B. Picard, B. Gouilleux, T. Lebleu, J. Maddaluno, I. Chataigner, M. Penhoat, F.-X. Felpin, P. Giraudeau, J. Legros, Oxidative neutralization of mustard-gas simulants in an on-board flow device with in-line NMR monitoring, Angew. Chem. Int. Ed. 56 (2017) 7568–7572, https://doi.org/10.1002/anie.201702744.

[49] N. Emmanuel, P. Bianchi, J. Legros, J.-C.M. Monbaliu, A safe and compact flow platform for the neutralization of a mustard gas simulant with air and light, Green Chem. 22 (2020) 4105–4115, https://doi.org/10.1039/D0GC01142H.

[50] Z. Chen, K. Ma, J.J. Mahle, H. Wang, Z.H. Syed, A. Atilgan, Y. Chen, J.H. Xin, T. Islamoglu, G.W. Peterson, O.K. Farha, Integration of metal–organic frameworks on protective layers for destruction of nerve agents under relevant conditions, J. Am. Chem. Soc. 141 (2019) 20016–20021.

[51] K. Ma, M.C. Wasson, X. Wang, X. Zhang, K.B. Idrees, Z. Chen, Y. Wu, S.-J. Lee, R. Cao, Y. Chen, L. Yang, F.A. Son, T. Islamoglu, G.W. Peterson, J.J. Mahle, O. K. Farha, Near-instantaneous catalytic hydrolysis of organophosphorus nerve agents with zirconium-based MOF/hydrogel composites, Chem Catal. 1 (2021) 721–733.

[52] S. Biswas, R. Gay, J. Bzdrenga, T. Soirot, N. Belverge, N. Taudon, X. Brazzolotto, M. Haouas, N. Steunou, J.P. Mahy, R. Ricoux, Detoxification of chemical warfare agents by a Zr-based MOF with high recycling ability at physiological pH, ChemNanoMat (2024) e202400132.

[53] A.R. Nandhini, M. Harshiny, S.N. Gummadi, Chlorpyrifos in environment and food: a critical review of detection methods and degradation pathways, Environmental Science: Process. Impacts 23 (2021) 1255–1277, https://doi.org/10.1039/D1EM00178G.

[54] A. Leskovac, S. Petrović, Pesticide use and degradation strategies: food safety, challenges and perspectives, Foods 12 (2023) 2709, https://doi.org/10.3390/foods12142709.

[55] M. Labaška, M. Gál, T. Mackulak, J. Švorec, J. Kučera, J. Helenin, V. Svitková, J. Ryba, Neutralizing the threat: a comprehensive review of chemical warfare agent decontamination strategies, J. Environ. Chem. Eng. (2024) 114243.

[56] S. Econdi, A. Caselli, S. Marchesi, F. Carniato, C. Bisio, M. Guidotti, Catalysis and decontamination: a versatile tool in the safe and sustainable degradation of chemical warfare agents, Eur. Phys. J. Plus 139 (2024) 782.

[57] M.C. de Koning, M. van Grol, T. Breijaert, Degradation of paraoxon and the chemical warfare agents VX, tabun, and soman by the metal–organic frameworks UiO-66-NH_2, MOF-808, NU-1000, and PCN-777, Inorg. Chem. 56 (19) (2017) 11804–11809, https://doi.org/10.1021/acs.inorgchem.7b01809.

[58] K. Kiaei, M.T. Nord, N.C. Chiu, K.C. Stylianou, Degradation of G-type nerve agent simulant with phase-inverted spherical polymeric-MOF catalysts, ACS Appl. Mater. Interfaces 14 (17) (2022) 19747–19755, https://doi.org/10.1021/acsami.2c03325.

[59] F. Carniato, G. Gatti, C. Bisio, An overview of the recent synthesis and functionalization methods of saponite clay, New J. Chem. 44 (2020) 9969–9980, https://doi.org/10.1039/D0NJ00253D.

[60] C.H. Zhou, Q. Zhou, Q.Q. Wu, S. Petit, X.C. Jiang, S.T. Xia, C.S. Li, W.H. Yu, Modification, hybridization and applications of saponite: an overview, Appl. Clay Sci. 168 (2019) 136–154, https://doi.org/10.1016/j.clay.2018.11.002.

[61] R.J.M.J. Vogels, J.T. Kloprogge, J.W. Geus, Synthesis and characterization of saponite clays, Am. Mineral. 90 (2005) 931–944, https://doi.org/10.2138/am.2005.1616.

[62] F. Carniato, C. Bisio, R. Psaro, L. Marchese, M. Guidotti, Niobium(V) saponite clay for the catalytic oxidative abatement of chemical warfare agents, Angew. Chem. Int. Ed. 53 (2014) 10095–10098, https://doi.org/10.1002/anie.201405134.

[63] S. Marchesi, M. Guidotti, L. Marchese, C. Evangelisti, F. Carniato, C. Bisio, Bifunctional europium(III) and niobium(V)-Containing saponite clays for the simultaneous optical detection and catalytic oxidative abatement of blister chemical warfare agents, Chem. Eur J. 27 (2021) 4723–4730, https://doi.org/10.1002/chem.202005454.

[64] D. Costenaro, C. Bisio, F. Carniato, S.L. Safronyuk, T.V. Kramar, M.V. Taran, M.F. Starodub, A.M. Katsev, M. Guidotti, Physico–chemical properties, biological and environmental impact of Nb–saponites catalysts for the oxidative degradation of chemical warfare agents, Chem. Select 2 (2017) 1812–1819, https://doi.org/10.1002/slct.201700042.

[65] C. Bisio, F. Carniato, C. Palumbo, S.L. Safronyuk, M.F. Starodub, A.M. Katsev, L. Marchese, M. Guidotti, Nanosized inorganic metal oxides as heterogeneous catalysts for the degradation of chemical warfare agents, Catal. Today 277 (2016) 192–199, https://doi.org/10.1016/j.cattod.2015.12.023.

[66] S. Marchesi, F. Carniato, M. Guidotti, M. Botta, L. Marchese, C. Bisio, Synthetic saponite clays as promising solids for lanthanide ion recovery, New J. Chem. 44 (2020) 10033–10041, https://doi.org/10.1039/C9NJ05983K.

[67] S. Marchesi, S. Nascimbene, M. Guidotti, C. Bisio, F. Carniato, Application of NMR relaxometry for real-time monitoring of the removal of metal ions from water by synthetic clays, Dalton Trans. 51 (2022) 4502–4509, https://doi.org/10.1039/D1DT04344G.

[68] O. Prieto, M.A. Vicente, M.A. Bañares-Muñoz, Study of the porous solids obtained by acid treatment of a high surface area saponite, J. Porous Mater. 6 (1999) 335–344, https://doi.org/10.1023/A:1009657312123.

[69] C. Tiozzo, C. Bisio, F. Carniato, M. Guidotti, Grafted non-ordered niobium-silica materials: versatile catalysts for the selective epoxidation of various unsaturated fine chemicals, Catal. Today 235 (2014) 49–57, https://doi.org/10.1016/j.cattod.2014.02.027.

[70] H. Zhu, Z. Zheng, X. Gao, Y. Huang, Z. Yan, J. Zou, H. Yin, Q. Zou, S.H. Kable, J. Zhao, Y. Xi, W.N. Martens, R.L. Frost, Structural evolution in a hydrothermal reaction between Nb2O5 and NaOH solution: from Nb2O5 grains to microporous $Na_2Nb_2O_6{\cdot}2/3H_2O$ fibers and $NaNbO_3$ cubes, J. Am. Chem. Soc. 128 (2006) 2373–2384, https://doi.org/10.1021/ja056301w.

[71] F. Tielens, T. Shishido, S. Dzwigaj, What do the niobium framework sites look like in redox zeolites? A combined theoretical and experimental investigation, J. Phys. Chem. C 114 (2010) 3140–3147, https://doi.org/10.1021/jp910956j.

[72] M. Thommes, K. Kaneko, A.V. Neimark, J.P. Olivier, F. Rodriguez-Reinoso, J. Rouquerol, K.S.W. Sing, Physisorption of gases, with special reference to the evaluation of surface area and pore size distribution (IUPAC Technical Report), Pure Appl. Chem. 87 (2015) 1051–1069, https://doi.org/10.1515/pac-2014-1117.
[73] M. Guidotti, R. Psaro, N. Ravasio, M. Sgobba, F. Carniato, C. Bisio, G. Gatti, L. Marchese, An efficient ring opening reaction of methyl epoxystearate promoted by synthetic acid saponite clays, Green Chem. 11 (2009) 1173–1178, https://doi.org/10.1039/B900863B.
[74] G.V.A. Martins, G. Berlier, C. Bisio, S. Coluccia, H.O. Pastore, L. Marchese, Quantification of brønsted acid sites in microporous catalysts by a combined FTIR and NH3-TPD study, J. Phys. Chem. C 112 (2008) 7193–7200, https://doi.org/10.1021/jp710613q.
[75] D. Liu, P. Yuan, H. Liu, J. Cai, D. Tan, H. He, J. Zhu, T. Chen, Quantitative characterization of the solid acidity of montmorillonite using combined FTIR and TPD based on the NH3 adsorption system, Appl. Clay Sci. 80–81 (2013) 407–412, https://doi.org/10.1016/j.clay.2013.07.006.
[76] C. Bisio, G. Gatti, E. Boccaleri, L. Marchese, L. Bertinetti, S. Coluccia, On the acidity of saponite materials: a combined HRTEM, FTIR, and solid-state NMR study, Langmuir 24 (2008) 2808–2819, https://doi.org/10.1021/la703308b.
[77] Q. She, M. Qiu, K. Li, J. Liu, C. Zhou, Acidic and basic sites on the surface of sodium montmorillonite active for catalytic transesterification of glycerol to glycerol carbonate, Appl. Clay Sci. 238 (2023) 106916.
[78] Y. Wang, Y. Muhammad, S. Yu, T. Fu, K. Liu, Z. Tong, X. Hu, H. Zhang, Preparation of Ca- and Na-modified activated clay as a promising heterogeneous catalyst for biodiesel production via transesterification, Appl. Sci. 12 (2022) 4667.
[79] D. Borah, D. Brahma, S. Roy, D. Basak, S. Agarwal, H. Saikia, Bentonite clay as a novel base heterogeneous catalyst in Knoevenagel Condensation of aldehydes with ethyl cyanoacetate in water, Results in Chemistry 7 (2024) 101238.
[80] B. Li, P. Sun, J. Zhen, W. Gong, Z. Zhang, W. Jia, G. Liang, L. Pan, pH-controlled UV−Vis sensing strategy for indirect, rapid detection of paraoxon based on molecular form conversion, Sensor. Actuator. B Chem. 348 (2021) 130715, https://doi.org/10.1016/j.snb.2021.130715.
[81] L.J. Michot, I. Bihannic, M. Pelletier, E. Rinnert, J.-L. Robert, Hydration and swelling of synthetic Na-saponites: influence of layer charge, Am. Mineral. 90 (2005) 166–172, https://doi.org/10.2138/am.2005.1600.
[82] M. Jiménez-Ruiz, E. Ferrage, A. Delville, L.J. Michot, Anisotropy on the collective dynamics of water confined in swelling clay minerals, J. Phys. Chem. A 116 (2012) 2379–2387, https://doi.org/10.1021/jp201543t.
[83] E. Tombácz, T. Nyilas, Z. Libor, C. Csanaki, Surface charge heterogeneity and aggregation of clay lamellae in aqueous suspensions, in: M. Zrínyi, Z.D. Hórvölgyi (Eds.), From Colloids to Nanotechnology, Springer, Berlin, Heidelberg, 2004, pp. 206–215, https://doi.org/10.1007/978-3-540-45119-8_35.
[84] M.P. Hart, D.R. Brown, Surface acidities and catalytic activities of acid-activated clays, J. Mol. Catal. Chem. 212 (2004) 315–321, https://doi.org/10.1016/j.molcata.2003.11.013.
[85] R.S. Murray, J.P. Quirk, The physical swelling of clays in solvents, Soil Science Soc of Amer J 46 (1982) 865–868, https://doi.org/10.2136/sssaj1982.03615995004600040039x.
[86] C. Wilson, N.J. Cooper, M.E. Briggs, A.I. Cooper, D.J. Adams, Investigating the breakdown of the nerve agent simulant methyl paraoxon and chemical warfare agents GB and VX using nitrogen containing bases, Org. Biomol. Chem. 16 (2018) 9285–9291, https://doi.org/10.1039/C8OB02475H.
[87] D. Millán, M. Rojas, R.A. Tapia, P. Pavez, Microwave-assisted nucleophilic degradation of organophosphorus pesticides in propylene carbonate, Org. Biomol. Chem. 18 (2020) 7868–7875, https://doi.org/10.1039/D0OB01620A.
[88] E. Ghanem, Y. Li, C. Xu, F.M. Raushel, Characterization of a phosphodiesterase capable of hydrolyzing EA 2192, the most toxic degradation product of the nerve agent VX, Biochemistry 46 (2007) 9032–9040, https://doi.org/10.1021/bi700561k.
[89] B. Garg, 31P solid-state NMR spectroscopy of adsorbed phosphorous probe molecules: acidity characterization of solid acid carbonaceous materials for catalytic applications, in: S.K. Sharma (Ed.), Handbook of Materials Characterization, Springer International Publishing, Cham, 2018, pp. 549–596, https://doi.org/10.1007/978-3-319-92955-2_14.
[90] A. Zheng, S.-B. Liu, F. Deng, 31P NMR chemical shifts of phosphorus probes as reliable and practical acidity scales for solid and liquid catalysts, Chem. Rev. 117 (2017) 12475–12531, https://doi.org/10.1021/acs.chemrev.7b00289.